Title: An approach to determine the features of dental X-ray images based on the fractal dimension

Author: Ireneusz Gościniak, Krzysztof Gdawiec, Krzysztof Woźniak, Monika Machoy

Citation style: Gościniak Ireneusz, Gdawiec Krzysztof, Woźniak Krzysztof, Machoy Monika. (2021). An approach to determine the features of dental X-ray images based on the fractal dimension. "Procedia Computer Science" Vol. 192 (2021), s. 1856-1865, doi 10.1016/j.procs.2021.08.191

Available online at www.sciencedirect.com

ScienceDirect

Procedia Computer Science 192 (2021) 1856–1865

Procedia Computer Science

www.elsevier.com/locate/procedia

25th International Conference on Knowledge-Based and Intelligent Information & Engineering Systems

An Approach to Determine the Features of Dental X-ray Images Based on the Fractal Dimension

Ireneusz Gościniak[a,*], Krzysztof Gdawiec[a], Krzysztof Woźniak[b], Monika Machoy[b]

[a]*Institute of Computer Science, University of Silesia, Będzińska 39, 41–200 Sosnowiec, Poland*
[b]*Department of Orthodontics, Pomeranian Medical University in Szczecin, Al. Powstańców Wlkp. 72, 70-111 Szczecin, Poland*

Abstract

Applications of the fractal dimension include the analysis and interpretation of medical images. The article presents a method for determining image features that are based on fractal dimension. In the proposed method, an optimization process (modified semi-multifractal optimization algorithm) creates a division into sub-areas similarly to a multi-resolution method. Using this division, a characteristic spectrum based on the fractal dimensions is calculated. This spectrum is applied to the recognition method of X-ray images of teeth. The obtained experimental results showed that the proposed method can effectively recognize such images.

Keywords: image analysis; multifractal analysis; image recognition; semi-multifractal algorithm; optimization

1. Introduction

Selecting good features that describe objects and matching measures is a central issue in image analysis [23]. Nowadays, the recognition of objects – based on these features and measures – is a very important task. The research on recognition methods is very intensive and diverse area of machine vision [23]. One of the approaches in finding features is multi-resolution analysis [2, 4, 21].

The multi-resolution analysis can be described as follows. A subdivision of the image that must fulfil the requirements regarding optimization issues is performed. Every sub-area is divided into proper squares or rectangles. The division process creates a tree. Every leaf of the tree has one of the following attributes: 1 – if the sub-area represents the object, 0 – if the sub-area is allocated in the background, [0, 1] – if the sub-area contains both: part of the object and the background.

* Corresponding author. Tel.: +48-694-366-102
E-mail address: ireneusz.gosciniak@us.edu.pl

1877-0509
10.1016/j.procs.2021.08.191

Only leaves with attributes within the range $[0, 1]$ are processed. The processing is limited by the precision – the minimal size of the sub-area.

Another popular approach for extracting features of objects is the use of fractal geometry. Fractals can create complex images using the self-similarity property [3]. Thanks to these properties, they can be used not only for image compression [3], but also for image recognition. Fractal features extraction is made using one of two approaches. In the first approach to obtain a fractal description of the object, the image is compressed using the fractal image compression algorithm, and then the features are extracted from the transformations created during the compression, e.g., proto-transformations [19], kernel density estimation of fractal coding parameters [26], mapping vectors [7], fractal dependence graph [8]. The second approach depends on the use of different kinds of fractal dimension, e.g., probability dimension [5], local fractal dimension [6, 17], 3D fractal dimension based on box counting, fractional Brownian motion and perimeter-area measurement [15].

The wide range of fractal analysis used in medicine is discussed in the literature review presented in [13]. The fractal analysis is widely used in cardiological and oncological applications and in ophthalmology, radiology, and dentistry. The bone tissue has a fractal construction. The fractal methods in dentistry are used to determine [13]: the changes in bone tissue regions, the evaluation of radiological images, implant stability, the different biomaterials influence on the character of bone remodelling, and it can be a descriptor of bone substitutes. However, the direct use of the fractal dimension is not suitable, because the appropriate quality of the analysed images must be obtained. It seems to be difficult for X-ray images.

Evolutionary algorithms are a group of algorithms inspired by nature. They are often applied to solve various two-dimensional problems. A fractal algorithm is a very interesting approach to global optimization [22] – it creates a fractal during the optimization process. The proper divisions of 2D space can create a deterministic multi-fractal, as shown in [20]. In [11], a semi-multifractal optimization algorithm that creates four collections of divisions was introduced. Four fractal dimensions representing a characteristic spectrum are calculated by using these collections.

In the literature, one can find many different approaches to dental X-ray images matching. Teeth contours are one of the most frequently used approaches [12, 14, 28]. Other interesting feature extraction methods of dental X-ray images are: signed feature histogram and keypoint detection [27] and the use of forcefield energy function on the tooth image and Fourier descriptors of the contour of the tooth [16]. In this paper, the characteristic spectrum obtained using the semi-multifractal optimization algorithm is used for the feature extraction. At first, a modification of the semi-multifractal optimization algorithm presented in [11] is proposed. Then, it is shown how to use the obtained characteristic spectrum for dental X-ray object recognition.

The remaining part of the paper is organized as follows. Section 2 introduces the proposed modifications of optimization algorithm. Next, Sec. 3 introduces image processes known in the literature. Then, in Sec. 4 a discussion on the use of automatic tuning of the algorithm is conducted. Moreover, a new recognition method that is based on the characteristic spectrum is introduced. Experimental verification of the proposed method is made in Sec. 5. Finally, Sec. 6 presents short concluding remarks.

2. Modifications of the optimization algorithm

There are many similarities between algorithms in the group of evolutionary algorithms. Heuristics (mostly metaheuristics) determine the behaviour of these algorithms. The immune algorithms are examples of such algorithms – the clonal selection algorithm deserves special attention. The immune algorithm has interesting properties that make this algorithm very effective [9]. In the subsequent iterations, the group of particles (antibodies) in the interaction with the environment (an antigen) produces mutated clones. The selected best-adapted (to the antigen) clones are a group of antibodies in the next iteration. The distribution of the particles in the solutions space depends on the algorithm operation and the environment function. Fractal and multifractal analysis of particles distribution (in relation to the immune algorithm) are proposed in [10]. The method from [10] shows a high efficiency – the fractal dimension and multifractal spectrum show changes in particles distribution. Representations of particles that implement specific image division rules, which have similar behaviour as in the immune algorithm are proposed in [11] – this method allows to determine the characteristic spectrum based on the fractal dimension. The production of clones (Fig. 1) is limited by the rules: $A \rightarrow (B, C)_{(4)}$, $B \rightarrow (D, A)_{(2)}$, $C \rightarrow \{(B, B)_{(1)}, (A, D)_{(2)}\}$, $D \rightarrow (A, A)_{(1)}$ (the number of produced clones is given in brackets).

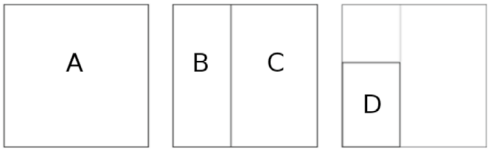

Fig. 1. Shapes of clones.

It results in obtaining four collections of elements that differ in scale – it gives the possibility to determine four fractal dimensions constituting the characteristic spectrum.

The operation of the Semi-Multifractal Optimization Algorithm (presented in Algorithm 1) can be described as follows:

1. The creation of a set of antibodies and evaluation[1].
2. The selection of an active antibody.
3. Clones production (by using active antibody), mutation and evaluation[2].
4. The active antibody is replaced by the best clone.
5. Repeat from step 2 up to the stop criteria are reached.

The evaluation[1] and evaluation[2] are functions of evaluation of antibodies and clones, respectively.

Algorithm 1: Semi-Multifractal Optimization Algorithm

Data: second is when two objects are separate instances in memory but have the same value. What t **Ab** – set of antibodies; Ab – an antibody ($Ab \in \mathbf{Ab}$); Ab^* – a selected antibody ($Ab^* \in \mathbf{Ab}$); **C** – set of clones; C – a clone ($C \in \mathbf{C}$); $\mathbf{C}^m$ – set of mutated clones; C^m – a mutated clone ($C^m \in \mathbf{C}^m$, $C^m \equiv \{Ab_1, Ab_2\}$); C^{*m} – a selected mutated clone ($C^{*m} \in \mathbf{C}^m$)

Input: Ag – an antigen ($f()$ – a solving problem); n_{Ab} – the number of antibodies; n_C – the number of clones;

Output: the best solution.

Ab $\longleftarrow$ initialise set of antibodies;
repeat
  $Ab^* \longleftarrow$ selection of $Ab \in$ **Ab** using roulette's well;
  C $\longleftarrow$ produces n_C clones of Ab^*;
  $\mathbf{C}^m \longleftarrow \{\forall C \in \mathbf{C}\ C$ is mutated and evaluated depending on Ag$\}$;
  $C^{*m} \longleftarrow$ select the best $C^m \in \mathbf{C}^m$;
  Ab $\longleftarrow$ (**Ab** $\setminus \{ Ab^* \}) \cup \{ C^{*m} \}$;
until stop criteria are not reached;
return Ab;

The algorithm controls the division of the solution space. This process produces four collections of figures differing in size (scale), see paper [11]. The differences between algorithms mostly result from the function of selection and evaluation. They decide on the algorithm's effectiveness. The proposed algorithm differs from the algorithm presented in [11] in antibodies and clones evaluation function. The proposed functions have a much smaller number of parameters necessary to determine its shape. The selection of these parameters affects the distribution of divisions of the image. Parameters of the functions have been determined experimentally – by the algorithm tuning.

The function of clones evaluation $f_c : [0,1]^2 \to [0,1]$ can be described by the following formula

$$f_c(p_1, p_2) = 1 - \frac{f(p_1) + f(p_2)}{2}, \tag{1}$$

where $f : [0, 1] \to \mathbb{R}$ is given by

$$f(p) = \begin{cases} \dfrac{p - A}{B - A} & \text{if } A \leq p < B, \\ 1 & \text{if } B \leq p < C, \\ \dfrac{D - p}{D - C} & \text{if } C \leq p \leq D, \\ 0 & \text{if } p < A \vee p > D, \end{cases} \tag{2}$$

and $p, p_1, p_2 \in [0, 1]$ are the coefficients of adaptation (see description of multi-resolution), and $A \leq B \leq C \leq D$. An example of the evaluation function of clones is presented in Fig. 2a. The parameters defining this function are as follows: $A = 0$, $B = 0.5$, $C = 0.5$ and $D = 1$ (to obtain the symmetry of the function $C = 1 - B$). The clones selection controls the population development.

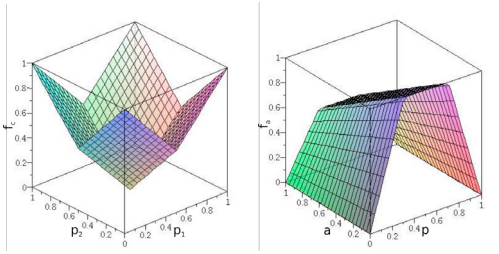

(a) (b)

Fig. 2. Fitness function for (a) clones and (b) antibodies evaluation.

Population improvement depends on antibodies selection. The selection is based on the antibodies function of evaluation. The size of sub-area and adaptation is taken into account in the evaluation. The function of evaluation $f_a : [0, 1]^2 \to \mathbb{R}$ is described by the following formula:

$$f_a(p, a) = f(p) \cdot l(a), \tag{3}$$

where $l : [0, 1] \to \mathbb{R}$ is given by $l(a) = 1 - a \cdot \sigma$ and $\sigma \in \mathbb{R}$ is the coefficient of sub-area impact, $a \in [0, 1]$ is the coefficient of sub-area (defined as the ratio of sub-area to the solution space area), $p \in [0, 1]$ is the coefficient of adaptation of produced antibody (p represents average shade, higher than the upper level or lower than the bottom level). The evaluation function f_a takes into account the evaluation f and the factor of the surface l. An example of the evaluation function of antibodies is presented in Fig. 2b. The parameters defining this function were as follows: $A = 0$, $B = 0.25$, $C = 0.75$ and $D = 1$ (for $B = C = 0.5$ the distribution of divisions is more uniform). Both evaluation functions f_c and f_a give a wide range of algorithm operation control.

3. Selected measures of image

Each image is represented as a set of points in 2D space. Image points can be grouped according to the specific rules. Analysis of image points and their groups using various methods gives a set of features describing the image. Selected methods of image analysis used in the following study are discussed below.

A histogram of the image gives a graphical representation of the levels (tones) distribution in a digital image [1]. Using this information, the image can be divided into two parts representing the background and the object. It can also be used to compare the quality of the images.

Thresholding is an image processing method used, for instance, in image segmentation [25]. Using only two colours during the thresholding process of a grey scale image, a binary image is obtained. The object is represented by the white colour, whereas the background as the black colour. This type of thresholding is often called binarization. For finding the threshold value, one can use the histogram of the image [18].

Another image measure is the characteristic spectrum introduced in [11]. To obtain this spectrum, firstly the division of the image using a semi-multifractal optimization algorithm is applied. The process of image division creates four sets of areas. Each of the sets is a covering of the image by objects of a given scale. Then, the fractal dimension D is calculated for each set by using the coverage $A(\varepsilon)$ and the scale ε:

$$D_k = \lim_{\varepsilon \to 0} \frac{\log A(\varepsilon)}{\log \varepsilon}. \tag{4}$$

The set of fractal dimensions creates the characteristic spectrum and is characteristic for an image.

The distribution of elements in the image can be analysed by designating a multifractal spectrum [10]. It is a good comparative method that visualises the distribution of the elements and their grouping. The method for determining the multifractal spectrum has been used as described in [10]. Because this method has an auxiliary meaning (indicator – it is used to compare the distribution of objects in space) a detailed description is not given here. The interested reader can find the description in [10].

4. Application of the algorithm for image recognition

As mentioned in the previous section, the binarization thresholds can be determined based on the histogram. Different values of the threshold cause significant differences in the obtained result. Wrong values can cause a problem with the identification of the appropriate image features that enable its identification. The use of an optimization algorithm can solve this problem. In this section, the automatic tuning of the optimization algorithm is presented to isolate the characteristics that are important in identification. X-ray images of teeth were used for the study. The proposed algorithm can be used to determine tooth structure characteristics (dentition) or for identification purposes.

The proposed method is of a comparative nature, therefore the analysis was carried out for image pairs. The tuning of the algorithm involves choosing two levels at which the processing is performed. Levels should be selected so as to the characteristic shapes are covered with subdivisions. It can be observed that the tooth's shape will be traced at the border of the background. However, the characteristic elements inside the tooth are above this border.

The evaluation functions used in the experiments are presented in Fig. 2 and the σ parameter used to define the l function was equal to 0.5. A discussion showing the possibilities of choosing the algorithm parameters, and their impact on its behaviour is presented below. At this point, it should be noted that these parameters' values have a significant influence on the distribution of the subdivisions. Afterwards, an attempt to automatic selection of these parameters is presented.

Automatic tuning is based on the threshold that divides the image into the background and the object. The first level represents the average value of background tones, whereas the second represents the average value of the object's tones.

The binary images (obtained from the images presented in Fig. 3a and b) of a single tooth are shown in Fig. 3c and d. It is not difficult to notice that the binary images are different. The subdivisions of the images presented in Fig. 3a and b are shown in Fig. 3e and f. Levels selected during the automatic tuning for the subdivisions shown in Fig. 3e assume the following values: 0.25 and 0.56. The levels automatically selected for the subdivisions that are shown in Fig. 3f assume the following values: 0.31 and 0.65 (histograms are not similar – Fig. 4a).

The binary images (obtained from the images presented in Fig. 5a and b) with two teeth are shown in Fig. 5c and d. The subdivisions of the images are shown in Fig. 5e and f. Levels selected during the automatic tuning for the subdivisions shown in Fig. 5e assume the following values: 0.37 and 0.66. Furthermore, the levels automatically selected for the subdivisions shown in Fig. 5f assume the following values: 0.32 and 0.66. Due to the high similarity of the histograms (Fig. 4b), the calculated values of levels are similar.

The binary images (obtained from the images presented in Fig. 6a and b) with four teeth are shown in Fig. 6c and d. The subdivisions of the images presented in Fig. 6a and b are shown in Fig. 6e and f. Levels selected during the automatic tuning for the subdivisions shown in Fig. 6e assume the following values: 0.18 and 0.46. Moreover, the levels automatically selected for the subdivisions shown in Fig. 6f assume the following values: 0.14 and 0.42. Differences in the level values are caused by differences in the histograms (Fig. 4c).

(a) (b) (c) (d) (e) (f)

Fig. 3. Test images of one tooth (a and b), binary images of test images of one tooth (c and d) and automatic subdivisions of test images (e and f).

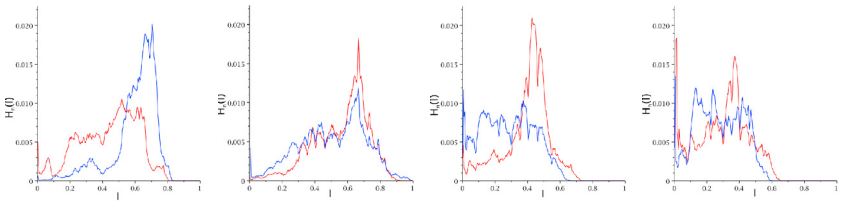

(a) for Fig. 3 (b) for Fig. 5 (c) for Fig. 6 (d) for Fig. 7

Fig. 4. Histograms of test images (for Figs. 3, 5, 6 and 7, a – red and b – blue).

(a) (b) (c) (d) (e) (f)

Fig. 5. Test images of two teeth (a and b), binary images of test images of two teeth (c and d) and automatic subdivisions of test images (e and f).

The binary images (obtained from the images presented in Fig. 7a and b) with two teeth are shown in Fig. 7c and d. The subdivisions of the images presented in Fig. 7a and b are shown in Fig. 7e and f. Levels selected during the automatic tuning for the subdivisions are shown in Fig. 7e assume the following values: 0.13 and 0.40. Furthermore, the levels automatically selected for the subdivisions shown in Fig. 7f assume the following values: 0.16 and 0.40. In this case, the calculated level values are similar because the histograms' similarity is high (Fig. 4d).

(a) (b) (c) (d) (e) (f)

Fig. 6. Test images of four teeth (a and b), binary images of test images of four teeth (a and b) and automatic subdivisions of test images (c and d).

The multifractal spectra for the images from Figs. 3–7 are shown in Fig. 8. It shows the differences in the distribution of divisions.

(a) (b) (c) (d) (e) (f)

Fig. 7. Test images of two teeth (a and b), binary images of test images of two teeth (c and d) and automatic subdivisions of test images (e and f).

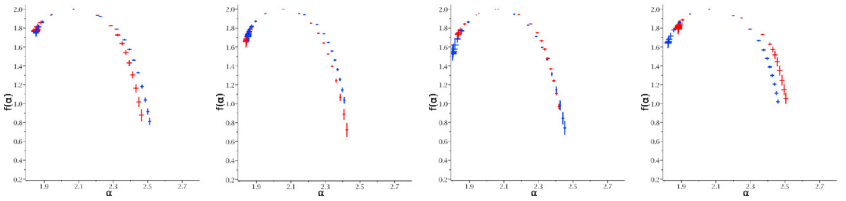

(a) for Fig. 3 (b) for Fig. 5 (c) for Fig. 6 (d) for Fig. 7

Fig. 8. Multifractal spectrum of automatic subdivisions of images (for Figs. 3, 5, 6 and 7).

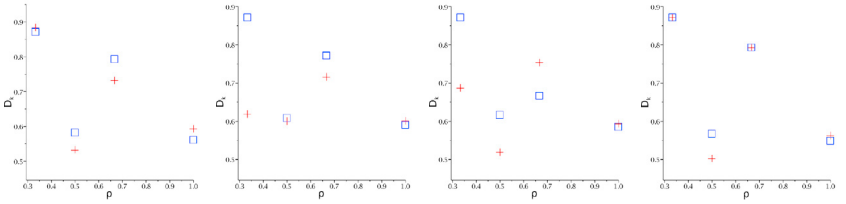

(a) for Fig. 3 (b) for Fig. 5 (c) for Fig. 6 (d) for Fig. 7

Fig. 9. Characteristic spectrum of automatic subdivisions of images (for Figs. 3, 5, 6 and 7).

The characteristic spectra for the images from Figs. 3–7 are presented in Fig. 9. The characteristic spectra presented in Fig. 9 show a considerable similarity of the compared images except for Fig. 9c. The shapes of the multifractal spectra shown in Fig. 8c are also very similar – significant differences occur in the location of the main coefficients: the fractal dimension and the information dimension. It is not difficult to observe a significant difference when comparing the images from Fig. 6a and b – these are clearly different objects.

An appropriate selection of the algorithm coefficients allows obtaining a similar spectral characteristic for different images. Whereas the proposed automatic tuning results in a more uniform distribution of image divisions. Automatic tuning gives satisfactory results. The determination of the average background and object level is a type of image normalization. Another way of selecting levels is also possible – the level of binarization is used as a low level in the next part of the study.

The discussion presented above shows a close relationship between the distribution of subdivisions and the image's individual character. To activate the characteristic features of the image, a scale-dependent mechanism for grouping subdivisions is introduced in the classifier. It is a mechanism for scaling the value of the determined spectral coefficient. A new group is created when the relative change in the division scale exceeds the specified s_i factor. So, in the classifier, n_g groups are created when the relative change in scale reaches the value s_1, and next the other groups are created when the relative change in scale reaches the value of s_2. Thus, for each spectral coefficient in the learning process, three grouping parameters are determined: n_g, s_1 and s_2. Spectral coefficients are computed using equation (4) assuming the maximum scale in the group.

The proposed recognition method of dental X-ray images is divided into the following steps:

1. Removing the test image from a set of images.
2. The classifier learning process.

3. Classification of the test image using nearest neighbour.

The test image classification is based on the sum of errors in the determination of spectral coefficients of the test image ($D_{At}, D_{Bt}, D_{Ct}, D_{Dt}$) and the ith image ($D_{Ai}, D_{Bi}, D_{Ci}, D_{Di}$) in the set (i.e., by using the Manhattan metric): $\varepsilon_i = |D_{Ai} - D_{At}| + |D_{Bi} - D_{Bt}| + |D_{Ci} - D_{Ct}| + |D_{Di} - D_{Dt}|$. The minimum error value ε_i indicates membership to the group.

5. Experiments

Experiments were performed on a database created by the authors. The database consists of 40 images divided into 10 classes (see Fig. 10). The classes are denoted with the letters of the alphabet A–J, and the number of images in each class is the following: A – 5, B – 5, C – 5, D – 5, E – 4, F – 4, G – 3, H – 4, I – 3, J – 2. The images in the database were created from 10 base images – one image per class. Each base image was changed by the following transformations: translation, rotation, scaling, reflection. Moreover, in some of the images, small changes to the tooth were added locally (see for example Fig. 10b and d).

Statistical data of the images from the database is presented in Tab. 1. For each of the images the following parameters were determined: the threshold level L_T, the average background level L_B, the average shade of object L_O, and characteristic spectrum coefficients D_A, D_B, D_C i D_D (letters in the subscript specify collections – see Fig. 1). Based on these results, it can be concluded that these images have very similar characteristics. The divisions obtained by the proposed algorithm are also presented in Fig. 10. These images reveal the characteristic elements of the subdivisions of images belonging to one group.

Table 1. Statistical parameters of the images.

Parameter	L_T	L_B	L_O	D_A	D_B	D_C	D_D
minimum	0.30	0.11	0.46	0.54	0.60	0.70	0.47
maximum	0.59	0.35	0.83	0.62	0.87	0.80	0.81
average	0.43	0.24	0.61	0.57	0.80	0.77	0.58
standard deviation	0.07	0.08	0.08	0.02	0.10	0.03	0.06
median	0.43	0.27	0.60	0.57	0.87	0.79	0.57

The use of these important image features requires learning the classifier. The obtained values of the coefficients are presented in Tab. 2. Because these parameters specify rules for creating groups, they are valid for all images in the set. Changes in the value of the s_1 and s_2 coefficients by several per cents do not affect the classifier's operation. At the same time, changes in the number of groups can significantly change the classifier's effectiveness.

Table 2. Parameters of the classifier.

Spectrum	n_g	s_1	s_2
D_A	3	0.65	0.80
D_B	3	0.70	0.65
D_C	1	0.90	0.50
D_D	4	0.45	0.35

To estimate the error rate of our recognition method the leave-one-out method [24] was used. The proposed recognition method correctly recognized 32 images, which gives an efficiency that equals to 80% and in consequence error of 20%. To better see the method's recognition capabilities, the positive predictive value matrix (PPV matrix) [25] was computed. The obtained PPV matrix is presented in Tab. 3.

From the obtained results, it is possible to see that only in the classes A, E, F, G and J the method correctly recognized all images in the class. For the other classes, one can observe that the method confuses objects of a given class with one or two classes' objects. The case with the confusion with one class was obtained for the C (the objects are confused with the object from class H), H (confusion with the C class) and I (confusion with the F class) classes. The misclassification of two classes occurred for an object of the B and D classes. The B class's confused objects were

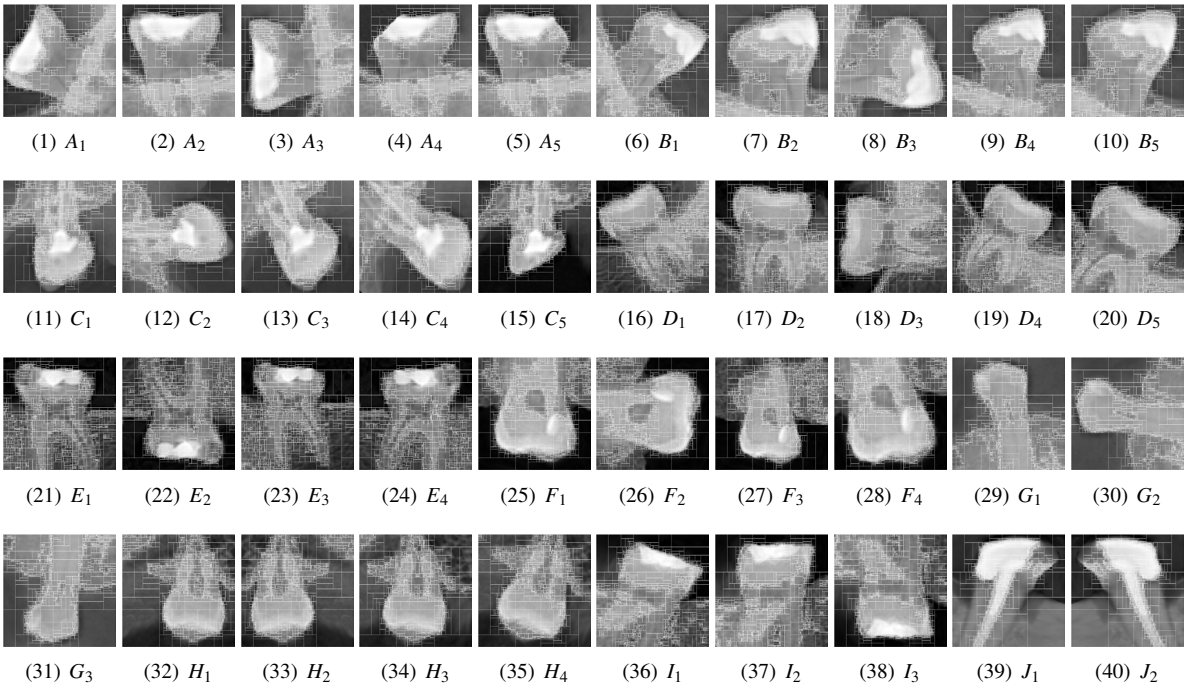

Fig. 10. Obtained subdivisions of the images from the database used in the experiments.

Table 3. Positive predictive values for test images.

Group	*A*	*B*	*C*	*D*	*E*	*F*	*G*	*H*	*I*	*J*
A	1.00	0.00	0.00	0.00	0.00	0.00	0.00	0.00	0.00	0.00
B	0.00	0.60	0.00	0.00	0.00	0.00	0.00	0.50	0.00	0.00
C	0.00	0.00	0.80	0.00	0.00	0.00	0.00	0.00	0.00	0.00
D	0.00	0.00	0.00	0.60	0.00	0.00	0.00	0.00	0.00	0.00
E	0.00	0.00	0.00	0.20	1.00	0.00	0.00	0.00	0.00	0.00
F	0.00	0.00	0.00	0.20	0.00	1.00	0.00	0.00	0.33	0.00
G	0.00	0.00	0.00	0.00	0.00	0.00	1.00	0.00	0.00	0.00
H	0.00	0.20	0.20	0.00	0.00	0.00	0.00	0.50	0.00	0.00
I	0.00	0.20	0.00	0.00	0.00	0.00	0.00	0.00	0.67	0.00
J	0.00	0.00	0.00	0.00	0.00	0.00	0.00	0.00	0.00	1.00

classified to the *H* and *I* classes, whereas the object from the *D* class to the *E* and *F* classes. The lowest PPV value that equals to 0.50, was obtained for objects of class *H*. Among the classes with the best representation (5 objects per class), the worst PPV value was obtained in the *B* and *D* classes for which this value was equal to 0.60.

6. Conclusions

A modification of the semi-multifractal optimization algorithm has been presented in this paper. The modification consisted in the use of evaluation functions that have a smaller number of parameters in comparison to the functions from [11]. Using this modified method and the characteristic spectrum a dental X-ray image recognition method is proposed. The obtained experimental results showed that the proposed method can effectively recognize X-ray images of teeth.

In our further work, the shapes of clones other than the ones used in the paper (Fig. 1) will be studied. This could lead to a decrease in recognition error. Moreover, other fractal features will be tried to combine into our method, e.g., features extracted from the fractal code obtained with the fractal compression.

References

[1] Bovik, A., 2009. The Essential Guide to Image Processing. Academic Press, New York.

[2] Ejbali, R., Jemai, O., Zaied, M., 2017. A multiresolution wavelet networks architecture and its application to pattern recognition. Pattern Recognition and Image Analysis 27, 949–510. doi:10.1134/S1054661817030105.

[3] Fisher, Y., 1995. Fractal Image Compression: Theory and Application. Springer-Verlag, New York, NY.

[4] Florindo, J., Bruno, O., 2013. Texture analysis by multi-resolution fractal descriptors. Expert Systems with Applications 40, 4022–4028. doi:10.1016/j.eswa.2013.01.007.

[5] Florindo, J., Bruno, O., 2014. Fractal descriptors based on the probability dimension: A texture analysis and classification approach. Pattern Recognition Letters 42, 107–114. doi:10.1016/j.patrec.2014.01.009.

[6] Florindo, J., Bruno, O., 2016. Local fractal dimension and binary patterns in texture recognition. Pattern Recognition Letters 78, 22–27. doi:10.1016/j.patrec.2016.03.025.

[7] Gdawiec, K., 2009. Shape recognition using partitioned iterated function systems, in: Cyran, K.A., Kozielski, S., Peters, J.F., Stańczyk, U., Wakulicz-Deja, A. (Eds.), Man-Machine Interactions. Springer, Berlin Heidelberg. volume 59 of *Advances in Intelligent and Soft Computing*, pp. 451–458. doi:10.1007/978-3-642-00563-3_48.

[8] Gdawiec, K., Domańska, D., 2011. Partitioned iterated function systems with division and a fractal dependence graph in recognition of 2D shapes. International Journal of Applied Mathematics and Computer Science 21, 757–767. doi:10.2478/v10006-011-0060-8.

[9] Gosciniak, I., 2008. Immune algorithm in non-stationary optimization task, in: 2008 International Conference on Computational Intelligence for Modelling Control Automation, pp. 750–755. doi:10.1109/CIMCA.2008.181.

[10] Gosciniak, I., 2017. Discussion on semi-immune algorithm behaviour based on fractal analysis. Soft Computing 21, 3945–3956. doi:10.1007/s00500-016-2044-y.

[11] Gosciniak, I., 2019. Semi-multifractal optimization algorithm. Soft Computing 23, 1529–1539. doi:10.1007/s00500-017-2874-2.

[12] Jain, A., Chen, H., 2004. Matching of dental X-ray images for human identification. Pattern Recognition 37, 1519–1532. doi:10.1016/j.patcog.2003.12.016.

[13] Leszczyński, P.and Sokalski, J., 2017. The use of fractal analysis in medicine: A literature review. Dental and Medical Problems 54, 79–83.

[14] Lin, P.L., Lai, Y.H., Huang, P.W., 2012. Dental biometrics: Human identification based on teeth and dental works in bitewing radiographs. Pattern Recognition 45, 934–946. doi:10.1016/j.patcog.2011.08.027.

[15] Lopes, R., Dubois, P., Bhouri, I., Bedoui, M., Maouche, S., Betrouni, N., 2011. Local fractal and multifractal features for volumic texture characterization. Pattern Recognition 44, 1690–1697. doi:10.1016/j.patcog.2011.02.017.

[16] Nomir, O., Abdel-Mottaleb, M., 2007. Human identification from dental X-ray images based on the shape and appearance of the teeth. IEEE Transactions on Information Forensics and Security 2, 188–197. doi:10.1109/TIFS.2007.897245.

[17] Obert, M., Hagner, S., Krombach, G., Inan, S., Renz, H., 2015. Fractal geometry enables classification of different lung morphologies in a model of experimental asthma. Fractals 23, 1550024. doi:10.1142/S0218348X15500243.

[18] Otsu, N., 1979. A threshold selection method from gray-level histograms. IEEE Transactions on Systems, Man, and Cybernetics 9, 62–66. doi:10.1109/TSMC.1979.4310076.

[19] Pazhoumand-dar, H., Yaghoobi, M., 2013. A new approach in road sign recognition based on fast fractal coding. Neural Computing and Applications 22, 615–625. doi:10.1007/s00521-011-0718-z.

[20] Pereira, M., Corso, G., Lucena, L., Freitas, J., 2005. A random multifractal tilling. Chaos, Solitons and Fractals 23, 1105–1110. doi:10.1016/j.chaos.2004.06.045.

[21] Rahman, R., Saha, S., 2009. Multi-resolution segmentation for object-based classification and accuracy assessment of land use/land cover classification using remotely sensed data. Journal of the Indian Society of Remote Sensing 36, 189–201. doi:10.1007/s12524-008-0020-4.

[22] Song, J., Qian, F., 2006. Fractal algorithm for finding global optimal solution, in: International Conference on Computational Intelligence for Modelling Control and Automation,and International Conference on Intelligent Agents,Web Technologies and Internet Commerce (CIMCA-IAWTIC'06), pp. 149–153. doi:10.1109/CIMCA.2006.100.

[23] Theodoridis, S., Koutroumbas, K., 2009. Pattern Recognition, 4th Edition. Academic Press, Burlington.

[24] Witten, I., Frank, E., 2005. Data Mining – Practical Machine Learning Tools and Techniques. 2nd Edn. Morgan Kaufmann Publishers, San Francisco, CA.

[25] Wu, Q., Merchant, F., Castleman, K., 2008. Microscope Image Processing. Academic Press, Burlington. doi:10.1016/B978-0-12-372578-3.00004-0.

[26] Xiaoqing, H., Qin, Z., Wenbo, L., 2013. A new method for image retrieval based on analyzing fractal coding characters. Journal of Visual Communication and Image Representation 24, 42–47. doi:10.1016/j.jvcir.2012.10.005.

[27] Zhang, Z., Ong, S., Zhong, X., Foong, W., 2016. Efficient 3D dental identification via signed feature histogram and learning keypoint detection. Pattern Recognition 60, 189–204. doi:10.1016/j.patcog.2016.05.007.

[28] Zhou, J., Abdel-Mottaleb, M., 2005. A content-based system for human identification based on bitewing dental X-ray images. Pattern Recognition 38, 2132–2141. doi:10.1016/j.patcog.2005.01.011.